

# Lawrence Berkeley National Laboratory

## LBL Publications

### Title

Green steel: design and cost analysis of hydrogen-based direct iron reduction

### Permalink

<https://escholarship.org/uc/item/80j7j7vm>

### Journal

Energy & Environmental Science, 16(10)

### ISSN

1754-5692

### Authors

Rosner, Fabian

Papadias, Dionissios

Brooks, Kriston

et al.

### Publication Date

2023-10-11

### DOI

10.1039/d3ee01077e


### Copyright Information

This work is made available under the terms of a Creative Commons Attribution License, available at <https://creativecommons.org/licenses/by/4.0/>

Peer reviewed

Cite this: *Energy Environ. Sci.*,  
2023, 16, 4121

## Green steel: design and cost analysis of hydrogen-based direct iron reduction†

Fabian Rosner,<sup>a</sup> Dionissios Papadias,<sup>b</sup> Kriston Brooks,<sup>c</sup> Kelvin Yoro,<sup>a</sup>  
Rajesh Ahluwalia,<sup>b</sup> Tom Autrey<sup>d</sup> and Hanna Breunig \*<sup>a</sup>

Hydrogen-based direct reduced iron (H<sub>2</sub>-DRI) is an alternative pathway for low-carbon steel production. Yet, the lack of established process and business models defining “green steel” makes it difficult to understand what the respective H<sub>2</sub> price has to be in order to be competitive with commercial state-of-the-art natural gas DRI. Given the importance of establishing break-even H<sub>2</sub> prices and CO<sub>2</sub> emission reduction potentials of H<sub>2</sub>-DRI, this study conducted techno-economic analyses of several design and operation scenarios for DRI systems. Results show that renewable H<sub>2</sub> use in integrated DRI steel mills for both heating and the reduction of iron ore can reduce direct CO<sub>2</sub> emissions by as much as 85%, but would require an H<sub>2</sub> procurement cost of \$1.63 per kg H<sub>2</sub> or less. When using H<sub>2</sub> only for iron ore reduction, economic viability is reached at an H<sub>2</sub> procurement cost of \$1.70 per kg, while achieving a CO<sub>2</sub> emission reduction of 76% at the plant site. System design optimization strategies around excess H<sub>2</sub> ratios in the DRI top gas and the H<sub>2</sub> recycle pressurization can further improve performance and economics. Low H<sub>2</sub> excess ratios are particularly attractive as they reduce pre-heating energy requirements and offer integration opportunities with static recycle ejectors if H<sub>2</sub> is supplied at sufficiently high pressure. The potential of utilizing the electric arc furnace off-gas is shown to be much more synergistic with H<sub>2</sub>-DRI than natural gas-DRI and can increase the break-even H<sub>2</sub> procurement cost by up to 7¢ per kg H<sub>2</sub>. Such findings are critical for setting technical performance criteria for H<sub>2</sub> supply and storage in the iron and steel sector.

Received 4th April 2023,  
Accepted 17th August 2023

DOI: 10.1039/d3ee01077e

rsc.li/ees

### Broader context

Substantially lowering greenhouse gas emissions from the iron and steel sector requires adopting new processes for iron ore reduction that will have impacts on facility energy efficiency, operation, and product cost. Hydrogen can be used as a reducing agent, and to serve high temperature thermal loads, allowing for the possible decoupling of the industry from coal and natural gas. However, the demand for low-carbon hydrogen from a single integrated steel mill could require giga-watts worth of renewable energy and electrolysis capacity. This work presents a detailed analysis of the use of hydrogen for making green steel, based on process modelling, and establishes price targets for hydrogen as well as guidance for process designs that can improve overall energy efficiency and integration.

## Introduction

Iron and steelmaking are essential parts of the U.S. economy, generating 87 million metric tonnes (MMT) of steel and \$88

billion in total revenue as of 2023.<sup>1</sup> These industries rely on fossil resources as heat sources and as reducing agents for the reduction of iron oxide in ore. Global iron and steelmaking are responsible for 8% of the global final energy demand and represent 7% of the energy sector's carbon dioxide (CO<sub>2</sub>) emissions.<sup>2</sup> The U.S. steel industry currently uses anywhere from 200 000–300 000 GW h of energy.<sup>3,4</sup> Energy efficiency improvements have been achieved over the past decades by increasing the recycling of steel, which consumes less energy per unit product,<sup>5,6</sup> and by lowering the energy consumption of iron and steelmaking.<sup>5</sup> These efficiency improvements tend to be motivated by high and uncertain energy prices but additionally contribute to reducing the direct CO<sub>2</sub> intensity of the industry,<sup>5</sup> where the average carbon intensity of crude steel

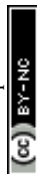
<sup>a</sup> Energy Analysis and Environmental Impacts Division, Lawrence Berkeley National Laboratory, Berkeley, CA 94720, USA. E-mail: hannabreunig@lbl.gov

<sup>b</sup> Transportation and Power Systems Division, Argonne National Laboratory, IL 60439, USA

<sup>c</sup> Energy and Environment Directorate, Pacific Northwest National Laboratory, Richland, WA 99352, USA

<sup>d</sup> Physical and Computational Sciences Directorate, Pacific Northwest National Laboratory, Richland, WA 99352, USA

† Electronic supplementary information (ESI) available. See DOI: <https://doi.org/10.1039/d3ee01077e>



production from iron ore is 1990 kg of CO<sub>2</sub> per metric tonne of steel compared with scrap steel recycling at 791 kg of CO<sub>2</sub> per metric tonne of steel.<sup>7</sup> While steel recycling has proven to be energy efficient and low in CO<sub>2</sub> emissions, primary steel will still be necessary to meet the growing demand for steel.<sup>6</sup>

Further minimizing CO<sub>2</sub> emissions of the steel industry has attracted significant interest over the years and numerous companies – accounting for 17% of the global steel production – have adopted net-zero-emission targets.<sup>8</sup> While technology upgrades and improvements in heat recovery can reduce CO<sub>2</sub> emissions,<sup>9</sup> these reductions become more incremental as technology matures. Carbon capture at steel facilities has proven to be challenging due to the high concentrations of carbon monoxide (CO), nitrogen (N<sub>2</sub>), and steam in the flue gases, as well as the unsteady nature of furnace off-gases (*i.e.* the electric arc furnace; EAF), calling for a reinvention of current steel production. As the majority of current steel facilities will reach their end of life by 2030 and require major reinvestments for refurbishment and relining, it is crucial to start investing in green steel technologies during the 2020s and avoid reinvestments into current steel facilities that will lock in new emissions for decades.<sup>10</sup> By using shaft furnaces, iron oxide can be directly reduced by methane (CH<sub>4</sub>)-derived syngas, a mixture of CO and H<sub>2</sub>. This can reduce direct CO<sub>2</sub> emissions by 61% compared to conventional coke-based iron production processes. When replacing CH<sub>4</sub> with renewable H<sub>2</sub>, direct CO<sub>2</sub> emission reductions of 97% are possible compared to the conventional blast furnace-basic oxygen furnace steelmaking process.<sup>11</sup> In a recent assessment of the steel industry, the International Energy Agency (IEA) further highlights the need for new low-emission steel technologies such as hydrogen-based direct reduced iron (H<sub>2</sub>-DRI).<sup>6</sup> Using renewable H<sub>2</sub> is currently still expensive, making the H<sub>2</sub>-DRI process highly dependent upon the availability of low-cost clean electricity and/or the implementation of a CO<sub>2</sub> emission tax;<sup>12</sup> nevertheless, H<sub>2</sub>-DRI shows advantages over other renewable carbon-based drop-in fuels.<sup>11</sup>

Preliminary comparisons of decarbonization pathways for iron and steelmaking suggest that H<sub>2</sub>-based iron oxide reduction in shaft furnaces has the greatest potential for lowering CO<sub>2</sub> emissions from primary steel production when using renewable electricity for H<sub>2</sub> production and serving ancillary power needs.<sup>7,13</sup> Other advantages of H<sub>2</sub>-based direct reduction of iron oxide include faster reaction kinetics compared to CO, which can reduce equipment size.<sup>14</sup> However, the endothermic nature of the iron oxide reduction reaction with H<sub>2</sub> makes the heat integration more challenging and a pre-heater for the H<sub>2</sub> is needed.<sup>15</sup> While this opens interesting heat integration options to improve the overall system efficiency, *e.g.* with the EAF off-gas (an often wasted resource), the high sensitivity of H<sub>2</sub>-based steel plants to the electrolyser efficiency typically leads to lower overall systems efficiencies when compared to the traditional blast furnace and basic oxygen furnace route.<sup>16</sup> Nevertheless, H<sub>2</sub>-based steel production offers an enormous CO<sub>2</sub> emission reduction potential and technologies for direct reduced iron (DRI) production using H<sub>2</sub> have been successfully demonstrated with no adverse effects on steel quality.<sup>17–19</sup>

This presents the opportunity for renewably generated H<sub>2</sub>, from sustainable regional energy resources, to be coupled with the steel industry. Due to the fluctuations in the availability of renewable power and the continuous nature of the steel-making process, there is a need for H<sub>2</sub> storage to supply cheap, low-carbon-emission H<sub>2</sub> continuously during operation.<sup>20</sup> A 1 000 000 tonnes-per-year steel facility, assuming an electrolysis-based facility with H<sub>2</sub> compression, requires approximately 60 kW h kg<sup>-1</sup>-H<sub>2</sub>, a wind or solar farm would need to be sized to 500 MW at a 100% capacity factor. In reality, power generation facilities of 1–2 GW are expected to account for renewable intermittency.

Today short-term compressed H<sub>2</sub> storage in steel plants – to shift the electricity use to off-peak hours – is shown to not offset the electrolyzer investment.<sup>21</sup> However, higher price fluctuations in a future grid with high renewable penetration are expected to make onsite H<sub>2</sub> storage a valuable asset increasing profit margins.<sup>22</sup> A drawback of compressed gas H<sub>2</sub> storage systems is their relatively high energy demand associated with gas compression. Thus, alternative H<sub>2</sub> storage systems, such as liquid organic H<sub>2</sub> carriers (LOHCs), are currently being considered for integration into steel facilities.<sup>23</sup>

Advantages of LOHCs include their easy handling and storage, as they are typically liquid at ambient temperature and pressure, which makes them highly compatible with current fossil fuel infrastructure. Liquid organic H<sub>2</sub> carriers can be centrally produced, to make use of the economies of scale, and transported to end-use locations. Methanol is shown to be an attractive option for such scenarios which offers a similar economic performance as compressed H<sub>2</sub> storage.<sup>24</sup> When thermally integrated with end-use H<sub>2</sub> applications, LOHCs are shown to be thermodynamically and economically advantageous over compressed H<sub>2</sub> storage solutions.<sup>25</sup> Particularly, the lower capital investment cost of LOHC systems are shown to economically outperform lined rock cavern H<sub>2</sub> storage at H<sub>2</sub>-DRI steel facilities.<sup>26</sup> In the same context, using methanol as LOHC is found to be more cost competitive compared to formic acid, ammonia, and perhydro-dibenzyltoluene, which suffer from large thermodynamic barriers for dehydrogenation and/or higher investment costs.<sup>27</sup>

The focus of this work is to characterize plausible hydrogen end use in iron and steelmaking in a manner that can inform coupling with H<sub>2</sub> generation and storage systems. In this study, break-even levelized cost of hydrogen (LCOH) targets for decarbonizing the steel industry with H<sub>2</sub>-DRI are established by comparing H<sub>2</sub>-DRI to the commercial natural gas-based direct reduced iron (NG-DRI) process. To enable this comparison, a detailed techno-economic analysis, supported by rigorous process modelling, is conducted. Detailed process models of integrated mills with NG-DRI and H<sub>2</sub>-DRI are developed to establish material balances, energy balances, balance-of-plant, direct and indirect CO<sub>2</sub> emissions, *etc.* This information is then used to derive the economic performance; whereby, the NG-DRI acts as the state-of-the-art reference case used to benchmark the H<sub>2</sub>-DRI performance. Detailed breakdowns of capital expenditure and cost-driving factors are discussed and their



respective impact on the levelized steel production cost (LSPC). By replacing the feedstock of the various NG users in the mill with H<sub>2</sub>, the decarbonization potential of the mill is evaluated together with its economic performance expressed in break-even LCOH. Additionally, key operating parameters of the H<sub>2</sub>-DRI process are studied to evaluate the economic impact of operating states upon the break-even LCOH and highlight opportunities for improving process design parameters. Specifically, EAF off-gas utilization is an important topic in this area as it contains substantial amounts of energy in the form of heat and CO, as well as smaller amounts of H<sub>2</sub>. The highly dynamic nature of this off-gas makes it difficult to utilize. In this work, we present dynamic simulations of the EAF off-gas to investigate its utilization potential in NG-DRI and H<sub>2</sub>-DRI applications, as well as shed light on the economic value of the respective utilization option.

In summary, while H<sub>2</sub>-DRI has been investigated in literature, this study provides a comprehensive techno-economic comparison of NG-DRI and H<sub>2</sub>-DRI configurations. While most studies integrate the electrolyzer into their analysis, it needs to be recognized that economical H<sub>2</sub>-production and economical H<sub>2</sub>-DRI operation are two connected but distinctively separate concerns. Along those lines, we provide insights into the pure H<sub>2</sub>-DRI economics, study H<sub>2</sub>-DRI operating parameters and their impact upon economics as well as derive break-even/target costs of H<sub>2</sub> to enable economical operation.

## Methodology

The system boundary is set around the physical plant site of an integrated DRI steel mill with EAF. The analysis includes the key processes shown in Fig. 1 and Fig. 2, as well as processes for EAF off-gas treatment, heat and electricity demand for ladle refining operations, and the cooling water system including evaporative cooling tower. Fuels, chemicals, and feedstocks,

such as electricity, NG, H<sub>2</sub>, carbon, lime, and iron ore pellets, are considered to be delivered to the plant site at their respective procurement costs. Emissions from their production are not included with those of the plant site but are accounted for as indirect emissions in the emission analysis. Direct emissions are emissions generated within the modelled system and cross the system boundary, which is drawn around the plant's stack. Other streams leaving the system boundary include the steel slab product, the slack, and the cooling tower blowdown. In this work, we study medium-sized integrated steel facilities with an annual production capacity of 1 162 000 metric tonnes of steel slabs, or an annual production of 1 046 000 metric tonnes considering downtime due to maintenance and other outages (90% capacity factor). An NG-based DRI facility with the same production capacity is used to benchmark the technical and economic performance of the H<sub>2</sub>-based DRI facility. Additional scenarios are modelled reflecting plausible variations on how H<sub>2</sub> is used in the facility, and how the EAF off-gas could be utilized; the former focusing on the use of H<sub>2</sub> to replace NG in heating applications, and the latter exploring opportunities for lowering the energy intensity of steel facilities. The reference integrated steel mill uses NG in four different processes, which could all in theory be served with H<sub>2</sub>: (I) the shaft furnace uses NG-derived syngas as reductant, (II) NG is used by the reformer as fuel for the firebox, (III) NG is used in the EAF and (IV) ladle refining processes.

All scenarios evaluated in the techno-economic analysis are developed in the process simulation software ProSim Plus.<sup>28</sup> We estimate total upfront investment, material and energy efficiency, and predict the maximum LCOH that is permissible in order to break even with the LSPC of the NG-DRI base case scenario. This means that a high break-even LCOH is desirable as it constitutes a scenario that is economically viable even if the cost of H<sub>2</sub> is high. This section provides an overview of the data and modelling approaches used to establish the performance metrics of the aforementioned technologies.

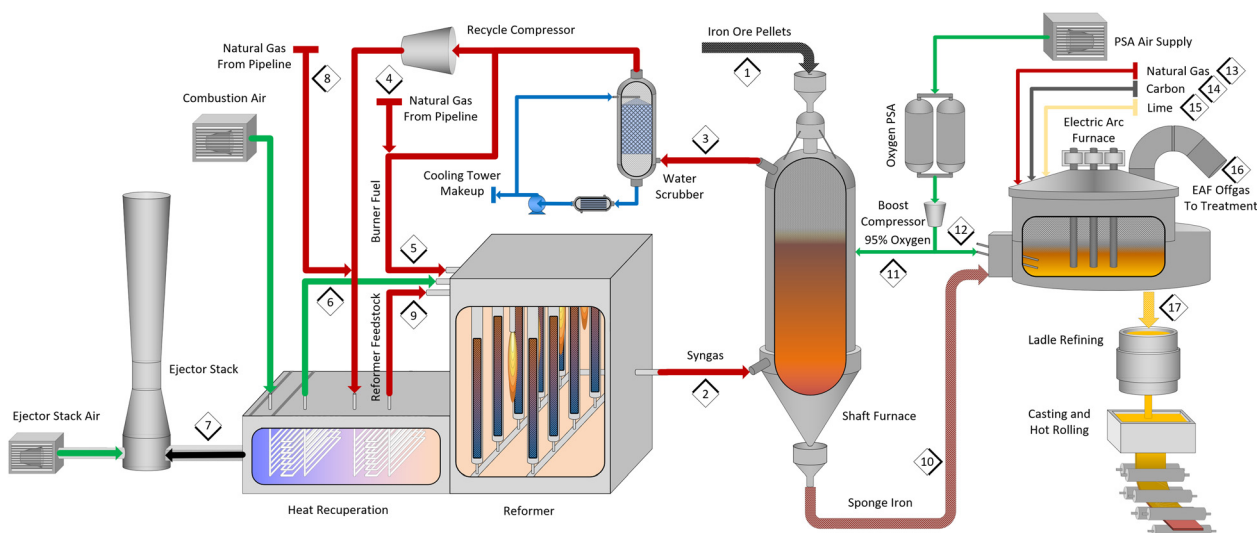


Fig. 1 Simplified flowsheet of the integrated natural gas-based DRI steel mill (NG-DRI-B).



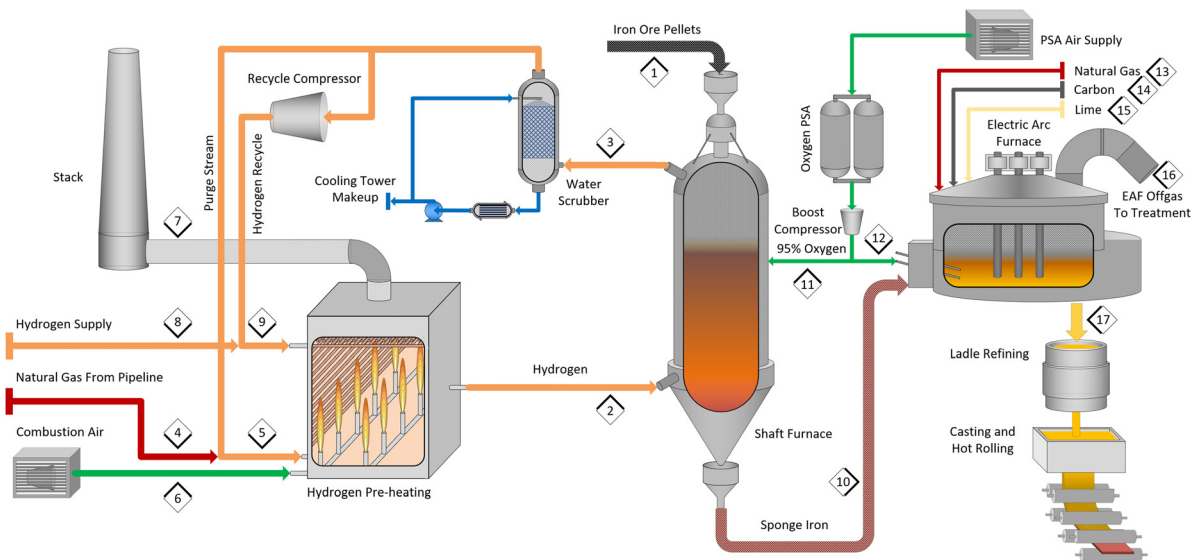


Fig. 2 Simplified flowsheet of the integrated hydrogen-based DRI steel mill ( $H_2$ -DRI-B).

### Direct reduced iron steel mill

The DRI plants investigated in this study are integrated mills with hot link, meaning that the sponge iron produced in the DRI process is not cooled to room temperature and is still hot when loaded into the EAF for further processing. A simplified flowsheet of the NG-DRI steel mill with its main process units and material streams is provided in Fig. 1. The corresponding state-point stream data with information about temperatures, pressures, flow rates, and composition can be found in the ESI<sup>†</sup> Table S1. A simplified flowsheet of the  $H_2$ -DRI steel mill with its main process units and material streams is provided in Fig. 2. The corresponding state-point stream data can be found in the ESI<sup>†</sup> Table S2.

### Natural gas reformer

The NG-based system, which acts as benchmark scenario, uses reformed NG or syngas in the shaft furnace as reducing agent for the iron oxide. The reformer operates on a mixture of NG and recycled syngas from the shaft furnace. The recycle scrubber temperature is adjusted to 70 °C to provide sufficient quantities of  $H_2O$  to the reformer<sup>15</sup> to minimize the risk of carbon deposition. Our gas stability analysis shows that operating the scrubber below 70 °C significantly decreases the water content in the recycle gas which increases the risk of carbon deposition in the downstream reformer. The reformer feedstock is pre-heated against the reformer's flue gas to a temperature of 500 °C prior to entering the reforming section. Inside the reformer, the steam reforming reaction, eqn (1), and water gas shift reaction, eqn (2), create a syngas high in  $H_2$  and CO, the reductants for reducing iron oxide to metallic iron. Reactions are reported at standard conditions, but occur over a range of temperatures in the furnace, which is captured in our simulations.

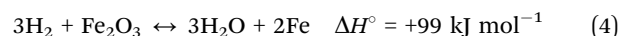
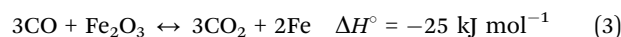


The catalyst used in this process is an alumina-supported nickel catalyst, as in Ko *et al.*<sup>29</sup> The operating conditions of reformers deployed in NG-DRI facilities differ from conventional steam methane reformers in feed composition, desired syngas  $CO/H_2$  ratio and operating pressure. Due to the integration with the shaft furnace, which typically operates at moderate pressures above atmosphere, the reformer operates at a pressure of 2.9 bar in order to minimize recycle compression work. The outlet gas (syngas) consists of 51 mol%  $H_2$ , 35 mol% CO, 8 mol%  $H_2O$ , 1 mol%  $CH_4$  and 5 mol%  $CO_2$ , which is in good agreement with literature values.<sup>15,30–32</sup>

The firebox operates with an excess air of 15% and maintains a thermodynamic temperature of greater than 1000 °C in the reforming section to facilitate the endothermic reforming reactions. To maximize the efficiency of the firebox, the combustion air is pre-heated to 500 °C against the flue gas before it enters the stack. Due to the high flue gas temperature, even after recuperation, an ejector stack is used.

### DRI shaft furnace

The syngas enters the shaft furnace at a temperature of 850 °C<sup>30,31,33,34</sup> where  $H_2$  and CO reduce the iron oxide stepwise to metallic iron. The metallization rate is assumed to be 94% for NG-DRI<sup>30–32,35</sup> and  $H_2$ -DRI.<sup>12,16,21</sup> The overall reducing reactions occurring in the shaft furnace are summarized in eqn (3) and (4):



At the same time syngas reactions such as the above-mentioned water gas shift reaction and carbon formation occur. The shaft furnace is loaded with iron ore pellets at the top and the feedstock slowly moves downward over time as it



heats up. On the way to the bottom of the furnace, the iron oxide comes in contact with hot CO and H<sub>2</sub> which reduces the Fe<sub>2</sub>O<sub>3</sub> first to Fe<sub>3</sub>O<sub>4</sub>, and FeO before converting it into metallic Fe. At the same time, CO and H<sub>2</sub> are converted to CO<sub>2</sub> and H<sub>2</sub>O. To mimic this behaviour, the reactor is modelled as a network of different heat exchange and reaction sections including the syngas reactions. To maintain a reducing atmosphere, excess CO and H<sub>2</sub> are needed. Higher excess ratios increase the chemical potential/driving force for the chemical reactions inside the shaft furnace; however, this increases the recycle stream and work associated with recompression. Typical top gas concentrations of the shaft furnace range from 33–49 mol% for H<sub>2</sub>, and 19–26 mol% for CO.<sup>30–32</sup> The temperature of the top gas leaving the shaft furnace ranges from 300–450 °C.<sup>30,31,34</sup> Thereafter, the top gas is quenched in a water scrubber to remove water produced by the iron ore reduction process as well as dust, and to lower the gas temperature for the recycle compressor. About 1/3 of the top gas is sent to the reformer's firebox where it is burned. This purge is necessary to eliminate the build-up of CO<sub>2</sub> and other compounds in the recycle.

The productivity of the shaft furnace can be improved by introducing high-purity O<sub>2</sub> into the furnace (or upstream of the shaft furnace) to raise the operating temperature of the shaft furnace, which improves reaction kinetics. Depending on the need to increase productivity, oxygen addition can vary greatly, and in this work a value at the lower end (0.1 kmol/metric tonne of sponge iron) has been chosen assuming the productivity of DRI and EAF is well balanced.<sup>35</sup>

### Electric arc furnace

The sponge iron leaves the shaft furnace at a temperature of 700 °C in this hotlink configuration and does not utilize methane injection at the bottom of the furnace to cool the sponge iron. The hot sponge iron is directly transferred to the EAF where it is melted using NG, carbon, and electricity as energy input to the EAF. EAF operating parameters are based on industrial operating data<sup>36,37</sup> and best practice values.<sup>38,39</sup> The EAF operates in batch mode; however, for simulation purposes, time-averaged values are used (at the process unit boundaries). At tapping, the liquid steel has a temperature of 1650 °C, and also the slag is assumed to be removed at this temperature. The average off-gas temperature was determined to be 1025 °C based on operational data available.<sup>36,37</sup> However, EAF operation can vary greatly based on steel type and debottlenecking efforts to increase productivity. Natural gas, carbon, oxygen, and lime consumption are based on best practice values<sup>38</sup> slightly modified to meet energy demands (cooling accounts for 10% of energy input).<sup>39</sup> Air leakage and average gas concentrations are based on industrial operating data.<sup>36,37</sup> The EAF off-gas is extracted from the EAF *via* water-cooled ducts and fed to a post-combustor where the off-gas is fully oxidized followed by further cooling, particle removal and venting using an induced draft fan. Ladle furnace operation, baghouse, casters, ladle heating and auxiliaries consume 22 kW h of natural gas per metric tonne of steel and 88 kW h of electricity per metric tonne of steel.<sup>38</sup>

### H<sub>2</sub>-based steelmaking

The H<sub>2</sub>-based DRI steel mill (Fig. 2) shares many similarities with the NG-based system. Sponge iron processing downstream of the shaft furnace remains unchanged except from some operating conditions to produce the same grade of steel (0.6 wt% C), *i.e.* more carbon is needed in the EAF since the sponge iron in the H<sub>2</sub>-DRI plant does not contain any carbon. The largest change compared to the NG-DRI plant is that the H<sub>2</sub>-DRI plant does not need a reformer; however, due to the endothermic nature of the iron ore reduction reaction with H<sub>2</sub>, the H<sub>2</sub> needs to be sufficiently pre-heated before entering the shaft furnace. This H<sub>2</sub> pre-heater is fueled by purged top gas from the shaft furnace (to avoid build-up of trace components such as N<sub>2</sub>), and makeup natural gas to meet the heat load. Moreover, the oxygen addition into the shaft furnace is increased to raise the operating temperature. Having both a pre-heater and O<sub>2</sub> injection increases operational flexibility. The size of the pre-heater, which pre-heats the H<sub>2</sub> to 775 °C is strategically chosen so that approximately 50% of the energy needed in the process is added to the shaft furnace directly (oxidation of H<sub>2</sub>) and the other 50% in the pre-heater to maximize flexibility and the ability to potentially buffer H<sub>2</sub> supply chain issues, which is particularly important if considering H<sub>2</sub> generation from 100% renewables. Furthermore, this design will allow the integration and utilization of the EAF off-gas a currently mostly wasted resource (more discussion on this in the Results and Discussion section). In the H<sub>2</sub>-base case, the top gas outlet contains approx. 30 mol% excess H<sub>2</sub> and has a temperature of 350 °C. This operating condition has been chosen based on the reduction potential of the reducing gas. Above approx. 500 °C, the shaft furnace inlet conditions are more reducing than in the NG-DRI scenario; however, outlet conditions of the H<sub>2</sub>-DRI scenario are less reducing than in the NG-DRI scenario.

### Design scenarios

In the following section, we provide an overview of the different design scenarios and sensitivity analysis studied. In the course of this analysis, we present scenarios and sensitivities to gauge the significance of certain H<sub>2</sub>-DRI operating parameters and to highlight critical areas in the research and development of H<sub>2</sub>-based DRI. As previously mentioned, the shaft furnace operation and various heat applications in the steel facility are switched from NG to H<sub>2</sub> to investigate break-even prices of H<sub>2</sub> and CO<sub>2</sub> emission reduction potentials. Furthermore, a scenario with electric H<sub>2</sub> pre-heating is included. Descriptions of the studied scenarios are summarized in Table 1.

Secondly, sensitivity studies are conducted. One for the cost of NG and electricity, which have been subject to large fluctuations over the past couple of years and are further location-dependent; and one for the H<sub>2</sub>-DRI-B and H<sub>2</sub>-DRI-T cases to investigate the impact of varying H<sub>2</sub> excess ratios in the shaft furnace. Due to limited data availability, it remains difficult to judge the exact amount of excess H<sub>2</sub> needed. This sensitivity analysis will shed light on the economic impact of this operating variable together with an alternate ejector-based top gas recirculation option.



Table 1 Design scenarios

Scenario	Description
NG-DRI-B	NG-DRI base case: NG use for syngas production, reformer heating, EAF heating, ladle heating.
NG-DRI-R	NG-DRI reformer case: NG use for syngas production, EAF heating, ladle heating. H <sub>2</sub> use for reformer heating.
NG-DRI-E	NG-DRI EAF case: NG use for syngas production, reformer heating, ladle heating. H <sub>2</sub> use for EAF heating.
NG-DRI-L	NG-DRI ladle case: NG use for syngas production, reformer heating, EAF heating. H <sub>2</sub> use for ladle heating.
NG-DRI-T	NG-DRI total case: NG use for syngas production. H <sub>2</sub> use for reformer heating, EAF heating, ladle heating.
H <sub>2</sub> -DRI-B	H <sub>2</sub> -DRI base case: H <sub>2</sub> use for shaft furnace. NG use for H <sub>2</sub> pre-heating, EAF heating, ladle heating.
H <sub>2</sub> -DRI-P	H <sub>2</sub> -DRI pre-heater case: H <sub>2</sub> use for shaft furnace, H <sub>2</sub> pre-heating. NG use for EAF heating, ladle heating.
H <sub>2</sub> -DRI-E	H <sub>2</sub> -DRI EAF case: H <sub>2</sub> use for shaft furnace, EAF heating. NG use for H <sub>2</sub> pre-heating, ladle heating.
H <sub>2</sub> -DRI-L	H <sub>2</sub> -DRI ladle case: H <sub>2</sub> use for shaft furnace, ladle heating. NG use for H <sub>2</sub> pre-heating, EAF heating.
H <sub>2</sub> -DRI-T	H <sub>2</sub> -DRI total case: H <sub>2</sub> use for shaft furnace, H <sub>2</sub> pre-heating, EAF heating, ladle heating.
H <sub>2</sub> -DRI-T <sub>EP</sub>	H <sub>2</sub> -DRI electric case: H <sub>2</sub> use for shaft furnace, EAF heating, ladle heating and electricity for H <sub>2</sub> pre-heating

Lastly, EAF off-gas utilization is studied using the NG-DRI-B and H<sub>2</sub>-DRI-T cases, and two exemplary EAF off-gases. EAF off-gas composition, temperature, and mass flow for EAF off-gas #1 and EAF off-gas #2 are shown in the ESI† Fig. S1 and S2. For each case (NG-DRI-B and H<sub>2</sub>-DRI-T), four sub-scenarios are investigated: (1) EAF off-gas #1 with single train EAF, (2) EAF off-gas #1 with two contracyclical EAF trains, (3) EAF off-gas #2 with single train EAF, (4) EAF off-gas #2 with two contracyclical EAF trains.

### Economics

The basis for the economic analysis is the year 2022. The LSPC is evaluated over an assumed 30 year plant operational period with a capital expenditure period of 3 years (33 years total). The total overnight cost is assumed to be 100% depreciable over 20 years at a 150% declining balance.<sup>40</sup> After-tax weighted average cost of capital for an investor-owned utility with 55% debt financing is 4.73% (real).<sup>40</sup> Tax rates are 21% (federal) and 6% (state).<sup>40</sup> This financing structure results in a capital charge factor (CCF) of 0.0776 and eqn (5) can be used to determine the LSPC.

$$\text{LSPC} = \frac{(\text{CCF})(\text{TOC}) + \text{OC}_{\text{fix}} + (\text{CF})(\text{OC}_{\text{var}})}{(\text{CF})(\text{MTPY})} \quad (5)$$

LSPC represents the cost of producing steel in the first year, calculated by taking into account factors such as the capital charge factor (CCF), the total cost of building the facility (TOC), fixed and variable annual operating costs (OC<sub>fix</sub> and OC<sub>var</sub>), the plant's capacity utilization (CF), and the expected annual production of steel at full capacity (MTPY). The TOC is the total overnight capital expenditure and includes the total plant cost (TPC) as well as pre-production costs, inventory capital, financing costs, land, and other owner's costs (for details see reference).<sup>41</sup>

Fixed operating costs (OC<sub>fix</sub>) include property tax and insurance at 2% of the TPC and operating labour. Operating labour for the integrated steel mill at the relevant scale is estimated with 51 skilled operators paid at an hourly rate of \$40.85 and 93 shift workers paid \$30.00 per hour. It is estimated that the labour burden accounts for 30% of the operating costs, and an additional 25% will be allocated for overhead expenses. Maintenance-related labour expenses make up 35% of the maintenance costs, and administrative and support labour

are 25% of the combined operating and maintenance labour costs.<sup>41</sup>

Variable operating costs (OC<sub>var</sub>) such as maintenance expenses are dependent on the availability of the plant. Other variable costs to consider include items like fuel, sorbents, and catalysts that are consumed during the production process. A summary of the consumables used in the steel mills is provided in Table 3 (for the analysis all costs are escalated to the year 2022 using an annual escalation factor of 3%). Particularly, the cost of NG and electricity have a substantial impact on the break-even cost of H<sub>2</sub> and vary not only over time but also by location. Just in the U.S. (excl. Hawaii) between late 2022 and early 2023, NG prices for industrial consumers varied from over \$60 per MW h in Massachusetts to less than \$10 per MW h in Texas. Similar differences are seen in industrial electricity prices with costs as high as \$180 per MW h and as low as \$55 per MW h. To cover the entire range of NG and electricity prices, the sensitivity study conducted in this study includes NG price ranges from \$63.69 per MW h to \$8.85 per MW h and electricity prices from \$180.00 per MW h to \$20.00 per MW h (considering future low-cost electricity which is a crucial part of achieving low-cost H<sub>2</sub> production).

Scaling costs to the relevant analysis year can be achieved *via* eqn (7). To obtain cost estimates at plant scale eqn (7) is used.

$$\text{SC} = \text{RC} \cdot (1 + \text{AER})^{\text{SY}-\text{RY}} \quad (6)$$

$$\text{SC} = \text{RC} \left( \frac{\text{SP}}{\text{RP}} \right)^u \left( \frac{\text{TS}}{\text{TR}} \right)^{0.9} \quad (7)$$

The scaled cost (SC) is determined by using the reference cost (RC), annual escalation rate (AER), scaled year (SY), and respective reference year (RY). To scale the equipment size, the scaling parameter (SP) and the reference parameter (RP) at reference scale are used along with the scaling exponent (*u*) which can be found in literature<sup>51</sup> for various types of plant equipment. The number of trains or quantity of equipment for the scaled plant is represented by TS, while TR represents the number of trains or quantity of equipment in the reference case. Additionally, an exponent of 0.9 is used to account for cost reduction when multiple units of the same equipment are purchased and installed. The expected accuracy of this methodology for capital cost estimation is between -30% to +50%, but scaling by more than a factor of two may increase the error



Table 2 Total plant cost correlations<sup>a</sup> (\$2022)

Process unit	Scaling parameter X	Correlation
EAF & casting	Liq. steel kg h <sup>-1</sup>	1132 370 X <sup>0.4560</sup>
Shaft furnace	Pig iron, kg h <sup>-1</sup>	49 080 X <sup>0.6538</sup>
Oxygen supply	O <sub>2</sub> product stream, kg h <sup>-1</sup>	30 622 X <sup>0.6357</sup>
Reformer	Furnace heat exchange, MW	4930 889 X <sup>0.6505</sup>
H <sub>2</sub> pre-heater	Furnace heat exchange, MW	228 860 X <sup>0.7848</sup>
Recycle compressor	Power, MW	6151 202 X <sup>0.7100</sup>
Cooling tower	Water, m <sup>3</sup> h <sup>-1</sup>	60 812 X <sup>0.6303</sup>
Electrical & instrumentation	Liq. steel, kg h <sup>-1</sup>	69 819 X <sup>0.5584</sup>
Buildings, storage, water service	Liq. steel, kg h <sup>-1</sup>	6320 X <sup>0.8000</sup>
Other miscellaneous cost	Liq. steel, kg h <sup>-1</sup>	174 548 X <sup>0.5583</sup>
Integrated NG-DRI steel mill (total)	Liq. steel, kg h <sup>-1</sup>	785 087 X <sup>0.5857</sup>
Integrated H <sub>2</sub> -DRI steel mill (total)	Liq. steel, kg h <sup>-1</sup>	800 884 X <sup>0.5647</sup>

<sup>a</sup> TPC includes EPC, process contingencies, project contingencies, etc.

margin. Capital cost estimates are based on values reported in literature<sup>51–55</sup> and ProSim economic evaluation. A reduced order model of the CAPEX is presented in Table 2.

### Direct and indirect CO<sub>2</sub> emissions

Direct emissions are emissions that occur within the system boundary defined earlier. These emissions originate from the use of fuels and feedstocks. The basis for direct emissions is the individual consumption rates to satisfy process specifications, heat loads, and chemistry. Indirect emissions are emissions associated with the production and procurement of materials used in the production process but occur outside the modelled system boundaries. Indirect CO<sub>2</sub> emissions are estimated from upstream life-cycle processes associated with raw material feedstocks and grid electricity based upon individual emission factors obtained from the EIA for grid electricity,<sup>56</sup> and from the Ecoinvent 3 database: electricity 386 kg<sub>CO2</sub> MW h<sup>-1</sup>, natural gas 0.44 kg<sub>CO2</sub> kg<sub>NG</sub><sup>-1</sup>, metallurgical coal 0.98 kg<sub>CO2</sub> kg<sub>C</sub><sup>-1</sup>, lime 0.05 kg<sub>CO2</sub> kg<sub>Lime</sub><sup>-1</sup>, iron ore mining 0.02 kg<sub>CO2</sub> kg<sub>Ore</sub><sup>-1</sup>, iron ore pelletizing 0.16 kg<sub>CO2</sub> kg<sub>Ore</sub><sup>-1</sup>.<sup>57</sup> The base assumption is that H<sub>2</sub> emissions are 0 kg<sub>CO2</sub> kg<sub>H2</sub><sup>-1</sup>, as suggested by the GREET model for solar H<sub>2</sub><sup>58</sup> and is used to represent upstream emissions from solar H<sub>2</sub> by Zang *et al.*<sup>4</sup> While emissions from solar and wind-powered H<sub>2</sub> generation from water electrolysis can be zero, indirect emissions from construction, maintenance, and transport activities can lead to CO<sub>2</sub> emissions. In accordance with the 45V tax credits, in the US, green H<sub>2</sub> must have CO<sub>2</sub> emissions of less than 0.45 kg<sub>CO2</sub> kg<sub>H2</sub><sup>-1</sup> in order to qualify for the full \$3 per kg<sub>H2</sub> tax credit. The impact of this emission value will be

further discussed in the following sections. The emission factors are summarized in Table 4.

## Results and discussion

### State-of-the-art natural gas DRI steel mill

The NG-DRI reference plant is analysed to determine benchmark values for efficiency, CO<sub>2</sub> emissions, and economic performance. In order to produce 1 045 000 metric tonnes of steel per year the shaft furnace processes 1 704 000 metric tonnes of iron ore annually, which consumes 11 388 000 GJ of natural gas. Additionally, 606 500 MW h of electricity are consumed whereby the EAF is responsible for over 62% of the electric load. This corresponds to a specific power consumption of 355 kW h per metric tonne of liquid steel whereby energy savings due to hotlink are 98 kW h<sup>-1</sup>, which is in good agreement with literature.<sup>38</sup> The carbon consumption in the EAF is 27 kg<sub>C</sub> per tonne<sub>Steel(lq.)</sub>, and lime consumption is 50 kg<sub>Lime</sub> per tonne<sub>Steel(lq.)</sub>. About 10% of the EAF's total energy is lost through the reactor walls<sup>39</sup> which is captured by the cooling system and dissipated in the cooling tower. The cooling tower consumes 1 337 000 metric tonnes of raw water per year, whereby 373 000 metric tonnes of cooling tower blowdown end up as surface discharge. Another disposal stream is the slag which amounts to 182 000 metric tonnes per year. Considering the total energy input, the thermal efficiency of this process is 54.3%-LHV. A summary of the energy balance and balance-of-plant power consumption is shown in the ESI† Table S3. Direct plant CO<sub>2</sub> emissions are 0.67 kg<sub>CO2</sub> kg<sub>Steel</sub><sup>-1</sup>. The EAF accounts for 0.12 kg<sub>CO2</sub> kg<sub>Steel</sub><sup>-1</sup> and the DRI process for

Table 3 Cost summary of fuel and consumables (based on U.S.)

Fuel/consumables	Value	Unit	Cost year	Ref.
Natural gas	33.85	\$ per MWh	2022	42
Electricity	93.40	\$ per MWh	2022	43
Iron ore pellet	130.00	\$ per tonne	2022	44 and 45
Slag disposal	30.00	\$ per tonne	2011	46
Solid waste disposal	200.00	\$ per tonne	2017	47
Raw water	0.44	\$ per m <sup>3</sup>	2011	46
Carbon	179.47	\$ per tonne	2019	48
Lime	100.00	\$ per tonne	2021	49
Reforming cat. (Ni–Al <sub>2</sub> O <sub>3</sub> )	17.52	\$ per litre	2014	50

Table 4 Emission factors of indirect emissions

Indirect emissions	Value	Unit	Region
Electricity	386	kg <sub>CO2</sub> MW h <sup>-1</sup>	US
Natural gas	0.44	kg <sub>CO2</sub> kg <sub>NG</sub> <sup>-1</sup>	US
Metallurgical coal	0.98	kg <sub>CO2</sub> kg <sub>C</sub> <sup>-1</sup>	Global
Lime	0.05	kg <sub>CO2</sub> kg <sub>Lime</sub> <sup>-1</sup>	Global
Iron ore mining	0.02	kg <sub>CO2</sub> kg <sub>Ore</sub> <sup>-1</sup>	Canada
Pelletizing	0.16	kg <sub>CO2</sub> kg <sub>Ore</sub> <sup>-1</sup>	Canada
Hydrogen	0 (0.45 <sup>a</sup> )	kg <sub>CO2</sub> kg <sub>H2</sub> <sup>-1</sup>	US

<sup>a</sup> US definition of green H<sub>2</sub> based on 45V tax credits.





0.55 kg<sub>CO2</sub> kg<sub>Steel</sub><sup>-1</sup>. The total (direct + indirect) CO<sub>2</sub> emissions of the plant are 1.32 kg<sub>CO2</sub> kg<sub>Steel</sub><sup>-1</sup>. Indirect emissions are dominated by the iron ore pelletizing process (0.26 kg<sub>CO2</sub> kg<sub>Steel</sub><sup>-1</sup>) followed by grid emissions (0.22 kg<sub>CO2</sub> kg<sub>Steel</sub><sup>-1</sup>). A breakdown of the emission sources and their contribution to the overall emissions is provided in Fig. 3. In comparison, the blast furnace-basic oxygen furnace route – where coke is used as reductant – produces 1.99–2.23 kg<sub>CO2</sub> kg<sub>Steel</sub><sup>-1</sup>,<sup>4,59</sup> whereby the blast furnace accounts for over 69% of the CO<sub>2</sub> emissions.<sup>59</sup>

The economic analysis shows that the TPC is \$795.5M which translates to a specific plant cost of \$685 per metric tonne of steel (based on annual production capacity). Considering pre-production costs, inventory capital costs, and other owner costs such as land, financing, *etc.*, the total overnight capital cost is \$1074.5M. Variable operating costs are \$414.9M per year (at 90% capacity factor), whereby the iron ore feedstock costs account for \$221.5M. Natural gas and electricity expenses are \$106.8M and \$56.6M, respectively. Other consumables such as water, carbon, and lime are responsible for \$12.1M. Maintenance materials add another \$10.8M annually and disposal costs for slag and other solids cost \$7.1M per year. The fixed operating costs account for an annual expenditure of \$110.6M, which is dominated by the operating labour with \$69.4M followed by tax and insurance costs of \$15.9M. Maintenance labour and administrative labour are \$6.4M and \$18.9M. The resulting LSPC is \$582.18 per metric tonne of steel. Hot-rolled steel traded at around \$670 per metric tonne towards the end of the year 2022.<sup>60</sup> However, in recent years, steel prices experienced large fluctuations due to market dynamics originating from tight supplies and high demand.<sup>61</sup> A breakdown of the individual cost-driving factors is shown in Fig. 3.

### Hydrogen in DRI steel mills

By switching the shaft furnace operation from natural gas-derived syngas to 100% renewable H<sub>2</sub> (H<sub>2</sub>-DRI-B), an onsite CO<sub>2</sub> emission reduction of 76.3% can be realized. Additionally, indirect emissions decrease by 14.3% primarily due to reduced NG use; however, increased carbon (coal)-use in the EAF

counteracts some of these effects. If a CO<sub>2</sub> emission factor of 0.45 kg<sub>CO2</sub> kg<sub>H2</sub><sup>-1</sup> is considered for green H<sub>2</sub> production, the specific indirect CO<sub>2</sub> emissions increase by 0.03 kg<sub>CO2</sub> kg<sub>Steel</sub><sup>-1</sup> resulting in a 9.6% reduction of indirect emissions. The great advantage of using H<sub>2</sub> as reductant is the reduced capital investment as the reformer becomes obsolete. This reduced capital investment as well as savings in operating costs (no catalyst needed) help to increase the break-even LCOH to \$1.70 per kg<sub>H2</sub> making this scenario an economically viable option long before the U.S. DOE target of \$1.00 per kg<sub>H2</sub> is reached (without any CO<sub>2</sub> credits).<sup>62</sup>

Next, we discuss replacing NG with H<sub>2</sub> as heat source. In the case of an NG-DRI, the ladle refining operation (NG-DRI-L) has little impact on the CO<sub>2</sub> emissions due to the small quantities of NG used in the process and only a CO<sub>2</sub> emission reduction of 0.6% can be achieved (direct emissions). To economically achieve this emission reduction, an LCOH of \$1.14 per kg<sub>H2</sub> or lower is needed. Replacing the NG used in the EAF for heating with renewable H<sub>2</sub> (NG-DRI-E) can lower the direct CO<sub>2</sub> emissions by 2.8% at a break-even LCOH of \$1.06 per kg<sub>H2</sub>. The amount of NG used in the reformer as heat input to the firebox is substantially higher and replacing this energy carrier with H<sub>2</sub> can reduce the direct CO<sub>2</sub> emissions of an integrated NG-DRI steel mill by 15.9% (NG-DRI-R). Similarly to the previous heat applications, the break-even cost of H<sub>2</sub> is \$1.19 per kg<sub>H2</sub>. This indicates that in order to economically replace NG with H<sub>2</sub> in heat applications in an NG-DRI steel mill, the LCOH needs to be close to the U.S. DOE target of \$1.00 per kg<sub>H2</sub>. Combining all these measures (NG-DRI-T), a reduction of direct CO<sub>2</sub> emissions of 19.4% is achievable at a break-even LCOH of \$1.16 per kg<sub>H2</sub>. Indirect emissions are only minimally impacted by replacing NG in heat applications with H<sub>2</sub>, a reduction of 0.02 kg<sub>CO2</sub> kg<sub>Steel</sub><sup>-1</sup> is achieved or 0.01 kg<sub>CO2</sub> kg<sub>Steel</sub><sup>-1</sup> if CO<sub>2</sub> emissions of 0.45 kg<sub>CO2</sub> kg<sub>H2</sub><sup>-1</sup> are associated with H<sub>2</sub> production.

Using H<sub>2</sub>-DRI and replacing NG as heat source for ladle refining, EAF, and H<sub>2</sub> pre-heating (H<sub>2</sub>-DRI-T case) can further the reduction of direct CO<sub>2</sub> emissions of the H<sub>2</sub>-DRI-B case from 76.3% to 84.9%. Indirect emissions are only reduced by

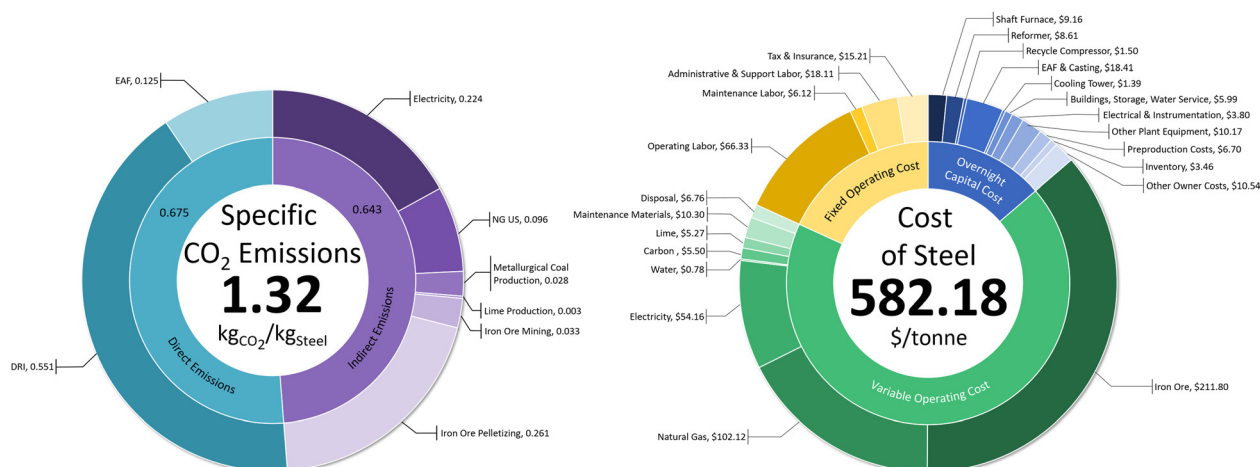


Fig. 3 Breakdown of carbon dioxide emissions (left) and levelized cost of steel (right) for the integrated NG-DRI steel mill.



0.01 kg<sub>CO2</sub> kg<sub>Steel</sub><sup>-1</sup> (0.02%) compared to the H<sub>2</sub>-DRI-B case and emissions from electricity generation and iron ore pelletizing account for over 73.5% of the total CO<sub>2</sub> emissions (direct + indirect). In the case where H<sub>2</sub> production is associated with CO<sub>2</sub> emissions of 0.45 kg<sub>CO2</sub> kg<sub>H2</sub><sup>-1</sup>, indirect CO<sub>2</sub> emission increase by 0.02 kg<sub>CO2</sub> kg<sub>Steel</sub><sup>-1</sup> (4.5%) over the H<sub>2</sub>-DRI-B case. As previously discussed, replacing NG in heat application is expensive compared to replacing NG as reductant in the shaft furnace; however, the large quantities of H<sub>2</sub> needed in the shaft furnace help to stabilize the break-even LCOH at \$1.63 per kg<sub>H2</sub> when adding H<sub>2</sub>-based heat applications in an H<sub>2</sub>-DRI steel mill. Hence, the most economical way to decarbonize DRI steel mills is to start with switching the shaft furnace operation from NG-derived syngas to renewable H<sub>2</sub>. Additional information on H<sub>2</sub>-DRI performance and economics can be found in the ESI.†

A sensitivity analysis of the NG cost and electricity cost shows that the break-even LCOH is highly dependent upon the NG cost, with high NG costs helping to increase the break-even LCOH. The high NG cost scenarios are representative for states such as Massachusetts and California and the low NG cost scenarios are more representative for states such as Texas and Oklahoma. The cost of electricity has relatively little impact upon the break-even LCOH. In general, higher electricity prices help to increase the break-even LCOH in the H<sub>2</sub>-DRI scenarios due to the slightly lower electricity consumption of the H<sub>2</sub>-DRI plants; however, in the scenario with electric H<sub>2</sub> pre-heater this

trend inverses as the electric heater substantially increases the electricity consumption in the H<sub>2</sub>-DRI-T<sub>EP</sub> case (higher than NG-DRI-B case). Currently, the H<sub>2</sub>-DRI-T<sub>EP</sub> case has a lower break-even LCOH than the H<sub>2</sub>-DRI-T case, but once electricity prices drop below \$51.10 per MW h this scenario is expected to be more economical (based on a LCOH of \$1.63 per kg, higher LCOHs will make this scenario economical at even higher costs of electricity). It is important to note here that an electricity price of \$51.10 per MW h is unlikely going to result in a LCOH of less than \$2 per kg, suggesting that electric H<sub>2</sub> pre-heating should be preferred over H<sub>2</sub>-fueled H<sub>2</sub> pre-heaters as long as steady electricity supply from renewable resources is not a concern. The results are summarized in Fig. 4 and Fig. S5 in the ESI.† The numeric values of this sensitivity analysis can be found in the ESI,† Table S12.

### Shaft furnace operation analysis

The amount of excess H<sub>2</sub> needed in the shaft furnace is an active area of research. The iron ore reduction potential of H<sub>2</sub> is greater than the reduction potential of syngas at shaft furnace inlet conditions explaining some of the fast reaction kinetics observed at high H<sub>2</sub> mole fractions.<sup>14</sup> However, at outlet conditions the opposite is true. At shaft furnace outlet conditions, the syngas has a higher reduction potential than the H<sub>2</sub>-DRI top gas. Nevertheless, operating temperature also plays a crucial role in process design and provides an opportunity to optimize operating conditions and the excess H<sub>2</sub> required. Fig. 5 shows the break-even cost of H<sub>2</sub> for a range of excess H<sub>2</sub> mole fractions in the shaft furnace top gas considering a constant H<sub>2</sub> reductant feed rate (Stream 8). As such, the H<sub>2</sub> utilization efficiency (reductant H<sub>2</sub> use in DRI/H<sub>2</sub> feed to DRI loop) of the shaft furnace remains constant at 82.3% throughout this sensitivity analysis (H<sub>2</sub> “losses” are due to purging and direct heating *via* O<sub>2</sub> injection). The red line represents the H<sub>2</sub>-DRI-B case with NG used to pre-heat the H<sub>2</sub> reductant fed into the shaft furnace, and the blue line represents an H<sub>2</sub>-DRI-T case that uses H<sub>2</sub> to pre-heat the H<sub>2</sub> for the shaft furnace. Using higher excess

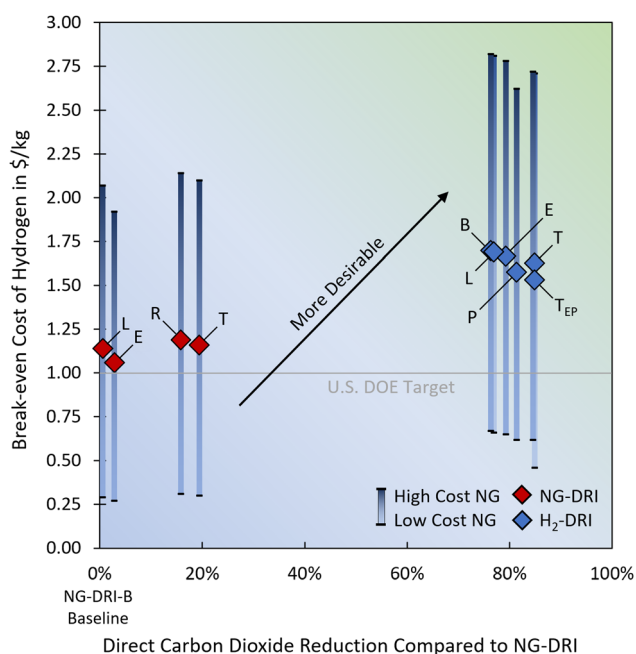


Fig. 4 Direct carbon dioxide emission reduction potential and associated H<sub>2</sub> break-even prices for the various NG consuming processes in an integrated DRI steel mill. The results of the NG price sensitivities are indicated by the blue bars for a range of \$63.69 per MW h (dark blue, representative for California and Massachusetts) to \$8.85 per MW h (light blue, representative for Texas and Oklahoma). The results of the electricity price sensitivities are presented in the ESI,† Fig. S5, together with the raw data for Fig. 4 and Fig. S5 (ESI†), which are presented in Table S12 (ESI†).

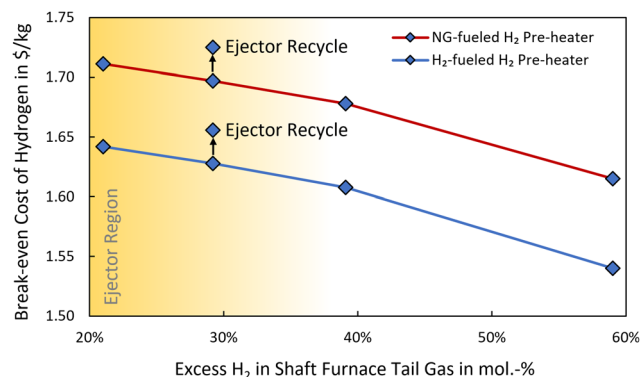


Fig. 5 Break-even cost of H<sub>2</sub> as function of excess H<sub>2</sub> in H<sub>2</sub>-DRI tail gas for NG-fueled H<sub>2</sub> pre-heater and H<sub>2</sub>-fueled H<sub>2</sub> pre-heater. At low excess ratios the recycle compressor can be replaced with an ejector if the primary H<sub>2</sub> is supplied at sufficiently high pressure indicated by the yellow region.



ratios, while maintaining the same tail gas temperature, has three major effects on the plant operation: (I) a higher  $H_2$  excess ratio leads to a larger  $H_2$  recycle stream increasing recycle compression power, (II) a larger recycle stream requires more energy for pre-heating, and (III) a larger feed stream into the shaft furnace reduces the  $O_2$  demand in the shaft furnace as the thermal inertia increases. While phenomena (I) and (II) lead to an economic performance decrease, some of this is counteracted by the phenomena described in (III). From an economic perspective it is desirable to operate the shaft furnace at low  $H_2$  excess ratios and past the 40 mol% mark a steeper decrease in economic performance is observed. By reducing the  $H_2$  excess from 59 mol% to 21 mol%, the break-even cost of  $H_2$  can be increased by 10¢ per kg of  $H_2$ . The absolute change remains the same for the NG-pre-heater case ( $H_2$ -DRI-B) and the  $H_2$  pre-heater case ( $H_2$ -DRI-T); however, considering the lower break-even cost in the  $H_2$ -DRI-T case this change is of higher relative importance with variations of  $-5.4\%$  (59 mol%  $H_2$  excess) and  $+0.9\%$  (21 mol%  $H_2$  excess) when compared to the base case scenario with 29 mol%  $H_2$  excess.

Lower  $H_2$  excess ratios have another advantage with respect to the plant design. Hydrogen excess ratios of approximately 30% and lower support the use of inexpensive static ejectors to facilitate the recycling of the unused excess  $H_2$ . If the primary  $H_2$  feedstock is available at sufficiently high pressures, *i.e.* 30 bar which is typical for PEM electrolyzers, this pressure can be utilized to recompress the recycle stream without the need for a mechanical compressor. In the case of ejector-based top gas recirculation, this need for high pressure  $H_2$  might also impact the economics and selection of suitable upstream  $H_2$  storage technologies. Capital cost savings on the compressor alone are over \$7.6M. Additionally, reducing the electrical load by 1.18 MW reduces the annual electricity costs by \$0.9M. As a result, using an ejector instead of a mechanical compressor can improve the break-even LCOH by another 3¢ per kg of  $H_2$ . While high-pressure  $H_2$  generation (around 30 bar) has become common practice, this pressure requirement might pose challenges for certain  $H_2$  storage technologies that might be used to buffer intermittencies of renewable electricity generation to ensure a steady supply of  $H_2$ .

### EAF off-gas utilization scenarios

The off-gases from the EAF contain a considerable amount of energy in the form of heat and chemical energy (CO,  $H_2$ ). Utilization of the off-gas has shown to be challenging because the off-gas composition not only varies substantially between different batches,<sup>63</sup> but also, during the different phases of operation (loading, heating, oxygen blowing, pre-tapping, tapping, *etc.*; see ESI<sup>†</sup>). While typical off-gases contain on average 7–12 mol% CO and 0–3 mol%  $H_2$ , momentary CO and  $H_2$  concentrations can be as high as 60 mol% and 20 mol%, respectively.<sup>36,64</sup> Due to these large fluctuations, EAF off-gases are commonly just cooled, oxidized, further cooled, and treated before the off-gas is eventually emitted into the atmosphere without utilizing any of its heat or caloric value. In the following section, the aforementioned two exemplary EAF off-gases are

used to study their utilization potential in the NG-DRI-B scenario and in the  $H_2$ -DRI-T scenario.

In the NG-DRI case, heat is needed in the firebox of the reformer to drive the endothermic reforming reactions, which requires a total heat input of approximately 202.1 MW-LHV. In the NG-DRI-B case, this energy input is partially provided by the DRI top gas purge and partially by a supplemental NG support fuel stream. In the scenario with EAF off-gas utilization, the off-gas is cooled, treated, and compressed (without oxidizing), and added into the reformer's firebox. The NG support fuel flow is then adjusted to meet the thermal load of the reformer. Due to the highly dynamic nature of this operation, the off-gas is analyzed dynamically in 30s intervals. Using EAF off-gas #1 (Fig. S1, ESI<sup>†</sup>) in the reformer firebox leads to an increase in fuel consumption by 1.7% confirming current industry practice as best practice scenario. Challenging for the utilization of the off-gas is its overall low heating value, which lowers the adiabatic flame temperature, making it more difficult to provide large quantities of high-temperature heat for the reforming reactions (over 1000 °C). Heating the non-combustible gases in the EAF off-gas to these temperatures adds a thermal penalty of 10.7 MW-LHV while the off-gas itself only contains 9.5 MW-LHV, leading to an overall increase in fuel consumption. Since most of the combustible gas output is present in the second half of the EAF batch operation, one could try to only use the EAF off-gas when its heating value reaches a certain threshold value; however, this would require more advanced control strategies as well as additional equipment for off-gas treatment during times when the off-gas is not sent to the reformer introducing new economic uncertainties.

Operating two EAFs in parallel, with their cycles 50% offset, can lead to a steadier off-gas; however, this does not change the time-averaged composition of the off-gas leading to the same 1.7% increase in fuel consumption. Off-gas #2, as shown in Fig. S2 (ESI<sup>†</sup>), has a higher CO mole fraction and lower mass flow rate per tonne of liquid steel compared to off-gas #1. As a result, the thermal penalty associated with gas heating is reduced to 6.3 MW-LHV. With an off-gas energy content of 9.4 MW-LHV, the NG support fuel consumption can be reduced by 4.2% in this scenario.

In the  $H_2$ -DRI-T case, heat is needed in the  $H_2$  pre-heater. The pre-heater requires 40.6 MW-LHV. In the  $H_2$ -DRI-T case, this energy is partially provided by the DRI top gas purge and partially by supplemental  $H_2$  fuel. Similarly, to the previously-discussed NG case, the EAF off-gas is cooled, treated, and compressed (without oxidizing), before it is combusted in the pre-heater firebox. To meet the heat load, the supplemental  $H_2$  fuel flow is adjusted as needed. Using EAF off-gas #1 in a single train setup shows a substantial 30.8% reduction in the pre-heater's fuel consumption. Since the  $H_2$  pre-heater operates in a much lower temperature window and can also make use of low-quality heat compared to the reformer ( $H_2$  is pre-heated from 55 to 775 °C), the penalty associated with heating non-combustible gases is less problematic and reduces to 2.5 MW-LHV. A new observation specific to the  $H_2$ -DRI pre-heater cases is that due to the high CO concentrations at certain times



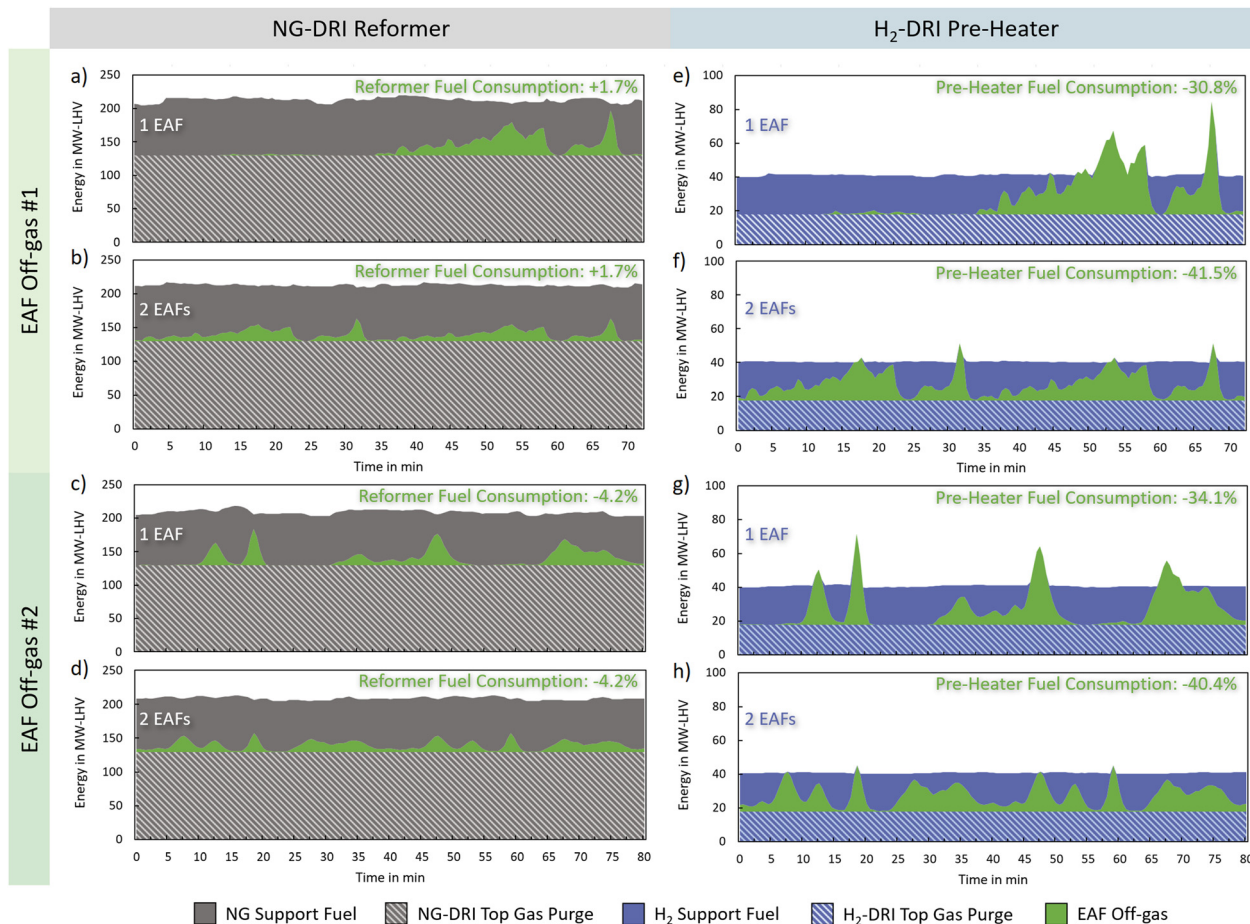


Fig. 6 EAF off-gas utilization analyses for the NG-DRI and H<sub>2</sub>-DRI cases. (a)–(d) show the fuel energy input (LHV) into the reformer firebox by fuel source and (e)–(h) show the fuel energy input (LHV) into the H<sub>2</sub> pre-heater by fuel source. Two different EAF off-gases are studied. Off-gas #1 is presented in (a), (b), (e) and (f) and off-gas #2 is presented in (c), (d), (g) and (h). For each of the combinations, 2 EAF setups have been considered. Single train EAF operation is presented in (a), (c), (e) and (g) and two-train operation with 50% cycle offset is presented in (b), (d), (f) and (h).

during the EAF operation and the relatively low heat demand of the pre-heater, some energy contained in the off-gas is wasted. Between minutes 50' and 58' as well as between minutes 66' and 68', the energy provided by the off-gas exceeds the heat necessary to pre-heat the H<sub>2</sub>-DRI feed as seen in Fig. 6e. To capture more of the caloric value contained in the EAF off-gas, the EAF operation can be performed in two parallel trains, with their cycles 50% offset. With this more balanced off-gas, excessive heating can be almost completely eliminated which increases the fuel savings in the pre-heater to 41.5% (Fig. 6f). Similar behavior is observed for off-gas #2 with pre-heater fuel savings ranging between 34.1–40.4%. An overview of the different EAF off-gas utilization scenarios is provided in Fig. 6.

The NG-DRI-B case shows that with EAF off-gas utilization the LSPC remains almost unchanged. With a 4.3% reformer fuel flow reduction in that scenario, the LSPC reduces by less than 0.1% resulting in a cost of \$581.70 per metric tonne of steel. The benefits of EAF off-gas utilization are much more apparent in the H<sub>2</sub>-DRI cases. EAF off-gas utilization in the H<sub>2</sub>-DRI-B case with NG as support fuel for the H<sub>2</sub> pre-heater can increase the break-even LCOH by 5 ¢ from \$1.70 to \$1.75 per kg of H<sub>2</sub>. This effect is even more pronounced if H<sub>2</sub> is used as

support fuel in the H<sub>2</sub> pre-heater (H<sub>2</sub>-DRI-T case), since H<sub>2</sub> is an expensive fuel for heating applications compared to NG. In that case, EAF off-gas utilization is able to increase to break-even LCOH by 7 ¢ from \$1.63 to \$1.70 per kg of H<sub>2</sub>. This confirms that the economic value of EAF off-gas utilization in NG-DRI is minimal at best; however, in H<sub>2</sub>-DRI, EAF off-gas utilization is shown to be a valuable asset to reduce support fuel consumption and improve economic performance.

## Conclusions

In this work, the authors investigated the performance of integrated steel mills with natural gas (NG)-direct reduced iron (DRI) and hydrogen (H<sub>2</sub>)-DRI to establish target costs for renewable H<sub>2</sub> production. The target values are break-even prices of H<sub>2</sub> that need to be achieved in order to maintain the identical levelized steel production cost (LSPC) as in the NG-DRI reference case.

The various NG users in the reference case were replaced with H<sub>2</sub>, showing that replacing NG-based heat applications in the NG-DRI mill with H<sub>2</sub> leads to a relatively small reduction in



CO<sub>2</sub> emissions while requiring a low cost of H<sub>2</sub> ranging from \$1.06–1.19 per kg of H<sub>2</sub>. However, switching the shaft furnace operation from NG to H<sub>2</sub>-shaft is shown to reduce capital costs, due to the omission of the reformer, leading to a break-even cost of H<sub>2</sub> of \$1.70 per kg, while reducing direct CO<sub>2</sub> emissions by 76.3%. Furthermore, converting the shaft furnace from NG to H<sub>2</sub> helps to stabilize the break-even cost of H<sub>2</sub> when switching the remaining NG heat applications to H<sub>2</sub>. As a result, a CO<sub>2</sub> emission reduction of 84.9% is reached at an H<sub>2</sub> break-even price of \$1.63 per kg of H<sub>2</sub>. After switching all NG users to H<sub>2</sub>, the largest CO<sub>2</sub> emissions originate from indirect emitters; predominately, the iron ore pelletizing process and electricity generation. This suggests that renewable electricity, and H<sub>2</sub>-DRI that can operate on iron ore fines rather than pellets are needed to further reduce CO<sub>2</sub> emissions. The third largest CO<sub>2</sub> source in H<sub>2</sub>-DRI (with H<sub>2</sub> heat applications) is direct emissions from the use of coking coal in the electric arc furnace (EAF).

Furthermore, lower H<sub>2</sub> excess ratios are shown to support higher break-even prices despite an increase in oxygen demand. Over a range of 21% to 59% H<sub>2</sub>-excess ratios, a 10¢ change in break-even cost of H<sub>2</sub> is observed. Additionally, excess ratios of around 30% or less allow the use of static ejectors to facilitate the H<sub>2</sub> recycle, eliminating the need for large recycle compressors if the primary H<sub>2</sub> supply pressure is sufficiently high, further boosting the break-even cost of H<sub>2</sub> by 3¢ per kg of H<sub>2</sub>.

Lastly, EAF off-gas utilization has been investigated. The results show that utilization of the off-gas in NG-DRI is difficult due to the low heating value and the need for high-temperature heat in the reformer, confirming that the flaring of EAF off-gases can be considered as best practice. However, for the H<sub>2</sub>-DRI scenario, it is found that due to the very different thermal load profile of the H<sub>2</sub>-pre-heater, EAF off-gas utilization can reduce the primary fuel consumption by up to 41.5% or up to 7¢ per kg of H<sub>2</sub> in terms of break-even costs.

## Author contributions

Conceptualization FR, HB, TA, KB, RA, DP; methodology FR, HB; software FR; validation FR, KB, AT, DP, HB; formal analysis FR, KB, KY, DP; investigation FR; resources HB; writing – original draft FR, HB, KB, TA, RA; writing – review & editing FR, HB; visualization FR; supervision HB; funding acquisition HB, TA, KB, DP, RA

## Conflicts of interest

There are no conflicts to declare.

## Acknowledgements

The authors gratefully acknowledge support from the U.S. Department of Energy under Contract No. DEAC02-05CH11231 with the Lawrence Berkeley National Laboratory, and with Pacific Northwest National Laboratory operated for

DOE by Battelle under Contract No. DE-AC05-76RL01830. The authors would like to acknowledge Vincent Chevrier for inputs on market direction, system simulation, and cost analysis. We thank Drs Ned Stenson, Jesse Adams, and Zeric Hulvey (DOE EERE) for their insights and guidance. The United States Government retains and the publisher, by accepting the article for publication, acknowledges that the United States Government retains a nonexclusive, paid-up, irrevocable, worldwide license to publish or reproduce the published form of this manuscript, or allow others to do so, for United States Government purposes.

## References

- 1 A. Moreno, US Industry NAICS report 33111, Jan. 2023, Accessed through IBISWorld.
- 2 International Energy Agency. *Iron and Steel Technology Roadmap*, 2020.
- 3 U.S. Energy Information Administration, First Use of Energy for All Purposes, Fuel and Nonfuel, 2021.
- 4 G. Zang, *et al.*, Cost and Life Cycle Analysis for Deep CO<sub>2</sub> Emissions Reduction for Steel Making: Direct Reduced Iron Technologies, *Steel Res. Int.*, 2023, **94**, 1–17.
- 5 E. Worrell, P. Blinde, M. Neelis, E. Blomen and E. Masanet, *Energy Efficiency Improvement and Cost Saving Opportunities; An ENERGY STAR Guide for Energy and Plant Managers*. LBNI-Report, 2010.
- 6 Energy Information Administration (EIA), *Tracking Iron and Steel, Tracking Report*, 2020, <https://www.iea.org/reports/tracking-iron-and-steel-2020>.
- 7 G. Zang, A. Elgowainy, P. Sun and B. Pallavi, *Decarbonization Pathways for Steelmaking, Summary Presentation to DOE Steelmaking Working Group*, Argon National Laboratory, September 2021.
- 8 L. Hermwille, *et al.*, A climate club to decarbonize the global steel, *Nat. Clim. Change*, 2022, **12**, 494–496.
- 9 Y. Sun, *et al.*, Decarbonising the iron and steel sector for a 2 °C target using inherent waste streams, *Nat. Commun.*, 2022, **13**, 2–9.
- 10 Agora Industry & Wuppertal Institute and Lund University, *Global Steel at a Crossroads Global Steel at a Crossroads. Why the global steel sector needs to invest in climate-neutral technologies in the 2020s*, 2021.
- 11 P. Fennell, J. Driver, C. Bataille and S. J. Davis, Cement and steel—nine steps to net zero, *Nature*, 2022, **603**, 574–577.
- 12 V. Vogl, M. Åhman and L. J. Nilsson, Assessment of hydrogen direct reduction for fossil-free steelmaking, *J. Cleaner Prod.*, 2018, **203**, 736–745.
- 13 M. Flores-Granobles and M. Saeys, Minimizing CO<sub>2</sub> emissions with renewable energy: A comparative study of emerging technologies in the steel industry, *Energy Environ. Sci.*, 2020, **13**, 1923–1932.
- 14 A. R. Costa, D. Wagner and F. Patisson, Modelling a new, low CO<sub>2</sub> emissions, hydrogen steelmaking process, *J. Cleaner Prod.*, 2013, **46**, 27–35.



- 15 K. Rechberger, A. Spanlang, A. S. Conde, H. Wolfmeir and C. Harris, Green Hydrogen-Based Direct Reduction for Low-Carbon Steelmaking, *Steel Res. Int.*, 2020, **91**, 2000110.
- 16 A. Bhaskar, M. Assadi and H. N. Somehsaraei, Decarbonization of the iron and steel industry with direct reduction of iron ore with green hydrogen, *Energies*, 2020, **13**, 758.
- 17 SSAB. HYBRIT. A new revolutionary steel making technology. <https://www.ssab.com/en/fossil-free-steel/hybrit-a-new-revolutionary-steelmaking-technology>.
- 18 J. Sampson Linde and Ovako heat steel with hydrogen. *GasWorld* <https://www.gasworld.com/linde-and-ovako-heat-steel-with-hydrogen/2018969.article> (2020).
- 19 V. Chevrier, MIDREX H2 and the transition to the hydrogen economy. in *Ironmaking with Alternative Reductants Webinar hosted by AIST*, 2020.
- 20 R. R. Wang, Y. Q. Zhao, A. Babich, D. Senk and X. Y. Fan, Hydrogen direct reduction (H-DR) in steel industry—An overview of challenges and opportunities, *J. Cleaner Prod.*, 2021, **329**, 129797.
- 21 A. Bhaskar, R. Abhishek, M. Assadi and H. N. Somehsaraei, Decarbonizing primary steel production: Techno-economic assessment of a hydrogen based green steel production plant in Norway, *J. Cleaner Prod.*, 2022, **350**, 131339.
- 22 M. Fishedick, J. Marzinkowski, P. Winzer and M. Weigel, Techno-economic evaluation of innovative steel production technologies, *J. Cleaner Prod.*, 2014, **84**, 563–580.
- 23 E. Southall and L. Lukashuk, Potential Deployment and Integration of Liquid Organic Hydrogen Carrier Technology within Different Industries, *Johnson Matthey Technol. Rev.*, 2022, **44**, 0–28.
- 24 D. D. Papadias, J. K. Peng and R. K. Ahluwalia, Hydrogen carriers: Production, transmission, decomposition, and storage, *Int. J. Hydrogen Energy*, 2021, **46**, 24169–24189.
- 25 M. Niermann, S. Drünert, M. Kaltschmitt and K. Bonhoff, Liquid organic hydrogen carriers (LOHCs) – techno-economic analysis of LOHCs in a defined process chain, *Energy Environ. Sci.*, 2019, **12**, 290–307.
- 26 J. Andersson and S. Grönkvist, A comparison of two hydrogen storages in a fossil-free direct reduced iron process, *Int. J. Hydrogen Energy*, 2021, **46**, 28657–28674.
- 27 J. Andersson, Application of liquid hydrogen carriers in hydrogen steelmaking, *Energies*, 2021, **14**, 1392.
- 28 ProSim Software and Services in Process Simulation ([www.prosim.net](http://www.prosim.net)). Getting started with ProSimPlus, ProSim Plus, Version 3.7.3.0, 2023.
- 29 K. D. Ko, J. K. Lee, D. Park and S. H. Shin, Kinetics of steam reforming over a Ni/alumina catalyst, *Korean J. Chem. Eng.*, 1995, **12**, 478–480.
- 30 B. Rami, H. Hamadeh, O. Mirgoux and F. Patisson, Carbon Impact Mitigation of the Iron Ore Direct Reduction Process through Computer-Aided Optimization and Design Changes, *Metals*, 2020, 1–12.
- 31 B. Rami, H. Hamadeh, O. Mirgoux and F. Patisson, Optimization of the Iron Ore Direct Reduction Process through Multiscale Process Modeling, *Materials*, 2018, **11**, 1–18.
- 32 D. R. Parisi and M. A. Laborde, Modeling of counter current moving bed gas-solid reactor used in direct reduction of iron ore, *Chem. Eng. J.*, 2004, **104**, 35–43.
- 33 K. S. Satyendra, MIDREX Process for Direct Reduction of Iron Ore, 2017.
- 34 Lockheed Martin. Ironmaking Process Alternatives Screening Study, Volume I: Summary Report Contents. I, (2000).
- 35 A. Ajbar, K. Alhumaizi, M. A. Soliman and E. Ali, Model-Based Energy Analysis Of An Integrated Midrex-Based Iron/Steel, *Chem. Eng. Commun.*, 2014, **201**, 37–41.
- 36 K. Gandt, T. Meier, T. Echterhof and H. Pfeifer, Heat recovery from EAF off-gas for steam generation: analytical exergy study of a sample EAF batch, *Ironmaking Steelmaking*, 2016, **43**, 581–587.
- 37 A. Thekdi, S. Nimbalkar, J. Keiser and J. Storey, *Preliminary Results from Electric Arc Furnace Off-Gas Enthalpy Modeling, Iron Steel Technology Conferrence Expositions*, Cleveland, OH, USA, 2015, pp. 1–15.
- 38 J. Stubbles, Energy Use in the U.S. Steel Industry: An Historical Perspective and Future Opportunities, Prep. US Dep, Energy, 2000.
- 39 J. A. T. Jones, *Electric Arc Furnace Steelmaking, Steelworks*, 2008.
- 40 U.S. Department of Energy/NETL, Quality Guidelines For Energy System Studies; Cost Estimation Methodology for NETL Assessments of Power Plant Performance, NETL-PUB-22580, 2019.
- 41 U.S. Department of Energy/NETL, Cost and Performance Baseline for Fossil Energy Plants Volume 1: Bituminous Coal and Natural Gas to Electricity, NETL-PUB-22638, 2019.
- 42 U.S. Energy Information Administration, United States Natural Gas Industrial Prices, 2022.
- 43 U.S. Energy Information Administration, Average Price of Electricity to Ultimate Customers by End-Use Sector, 2022.
- 44 U.S. Geological Survey, Iron Ore. Miner. Commod. Summ., 2022.
- 45 Z. Yu, Demand for seaborne iron ore pellet, concentrate continues to weaken, *Fastmarkets*, 2021.
- 46 U.S. Department of Energy/NETL, NETL Updated Costs (2011 Basis) for selected Bituminous Baseline Cases, DOE/NETL-341/082312, 2012.
- 47 Haulla, How Much Does Commercial Waste Collection Cost? [haulla.com](http://haulla.com), 2022.
- 48 Statistica, Coking coal price from 2012 to 2019, 2021.
- 49 Quicklime price, Made-in-China.com, 2021.
- 50 Zaubas Import Export Database, Katalco 57-4 Primary Reforming Catalyst., 2021.
- 51 D. R. Woods, *Rules of Thumb in Engineering Practice*, 2007.
- 52 Steelonthenet.com, Capital Investment Cost - Electric Arc Furnace, <https://www.steelonthenet.com/kb/steelmaking-capex-costs-dri-plant.html>.
- 53 Lockheed Martin, Ironmaking Process Alternatives Screening Study, Volume II: Appendix, 2000.
- 54 R. Šulc and P. Dítl, A technical and economic evaluation of two different oxygen sources for a small oxy-combustion unit, *J. Cleaner Prod.*, 2021, **309**, 127427.



- 55 U.S. Department of Energy/NETL, Cost and Performance Baseline for Fossil Energy Plants Volume 3a: Low Rank Coal to Electricity: IGCC Cases. DOE/NETL-2010/1399, 2011.
- 56 U.S. Energy Information Administration. How much carbon dioxide is produced per kilowatthour of U.S. electricity generation?, 2021, <https://www.eia.gov/tools/faqs/faq.php?id=74&t=11>.
- 57 G. Wernet, C. Bauer, B. Steubing, J. Reinhard, E. Moreno-Ruiz and B. Weidema, The ecoinvent database version 3 (part I): overview and methodology, *Int. J. Life Cycle Assess.*, 2016, **21**(9), 1218–1230.
- 58 Greenhouse Gases, Regulated Emissions, and Energy use in Transportation (GREET) Model; Argonne National Laboratory (ANL): Lemont, IL, USA, 2014. (accessed on February 22 2023).
- 59 A. Orth, N. Anastasijevic and H. Eichberger, Low CO<sub>2</sub> emission technologies for iron and steelmaking as well as titania slag production, *Miner. Eng.*, 2007, **20**, 854–861.
- 60 Phoenix Steel Service Inc. USA Steel Base Prices–Midwest. *Online* (2023).
- 61 MetalMiner. U.S. Steel Prices Surge As Supply Fails To Meet Demand. *OilPrice.com* (2023).
- 62 B. S. Pivovar, M. F. Ruth, D. J. Myers and H. N. Dinh, Hydrogen: Targeting \$1/kg in 1 Decade, *Electrochem. Soc. Interface*, 2021, **30**, 61–65.
- 63 M. Kirschen *et al.*, Off-gas measurements at the EAF primary dedusting system. *EEC Birmingham* (2005).
- 64 M. Kirschen, H. Pfeifer, F.-J. Wahlers and H. Mees, Off-Gas Measurements for Mass and Energy Balances of a Stainless Steel EAF. *59th Electr. Furn. Conf. Phoenix USA* (2001).

